tions. This comparison is given in Table IV. About 80–90% of the energy improvement found in going from simple Slater orbitals (with nonoptimized z_a's) to the exact HF values is obtained by using the optimized 11-STO basis. The additional improvement that can be obtained by going to very large basis sets is shown by Watson's[1] and by Clementi's[2] results. The former used a basis of 10 s-type STO's, 5 p-type STO's, and 4 d-type STO's. The latter used one more function of each symmetry type, a basis of 22 STO's in all. If we restrict ourselves to an 11-STO basis, significant improvement can only come about by removing the constraints imposed by the restricted HF method and by including relativistic effects.

PHYSICAL REVIEW VOLUME 165, NUMBER 1 5 JANUARY 1968

Photo-Ionization in the Soft x-Ray Range: Z Dependence in a Central-Potential Model

STEVEN TRENT MANSON* AND JOHN W. COOPER
National Bureau of Standards, Washington, D. C.
(Received 17 July 1967)

Using a one-electron model with a Herman-Skillman central potential, photo-ionization calculations have been performed which emphasize the soft x-ray spectral range (~100 eV to ~2 keV). The $M_{II,III}(3p)$ subshell was studied in Ar, Cu, and Ge, as well as the $M_{IV,V}$ $(3d)$ and $M_{II,III}$ in Kr, Rh, Xe, Eu, Au, and Fm in an effort to explain the combined Z and energy dependence of the photo-ionization cross sections for these subshells. In addition, calculations have been performed for $3s, 4s, 5s, 4p, 5p, 4d, 5d$, and $4f$ subshells in certain elements. The results, which are considerably different from the predictions of the hydrogenlike model, show certain regularities which are explained in terms of the potentials. Comparisons with experiment show that the model correctly predicts the gross spectral shape of photo-ionization cross sections, but the results are somewhat inaccurate in the vicinity of large absorption peaks. This calculation is considered to be a first approximation which can be improved by taking exchange into account more exactly and by including electron-electron correlation.

I. INTRODUCTION

RECENT experiments[1–3] have shown that in the soft x-ray region (i.e., excitation energies of ~100–2000 eV or wavelengths of ~100–6 Å) photoabsorption cross sections do not show the characteristic monotonic decrease above absorption edges which is typical of their behavior at higher energies. While the few detailed calculations that have been made[4–6] show that maxima in absorption need not correspond to absorption edges, not enough work has been done to determine in what energy ranges and for what elements maxima in photoabsorption may occur. The situation is further complicated since, with the exception of the rare gases, all photoabsorption measurements have been made in the soft x-ray range on materials either in the solid state or in gaseous chemical compounds. In the energy ranges just above each photoabsorption edge, band structure in the solid[7] or diffraction effects due to the presence of a number of atoms in a crystal lattice or molecule[8] are known to have a marked effect on the photoabsorption cross section. In the soft x-ray range it is not certain whether observed variations in photoabsorption cross sections are due to such effects or to the energy dependence of the atomic photo-ionization cross section itself.

At higher energies (>10 keV), reliable estimates of absorption coefficients may be obtained by assuming that the dominant absorption mechanism is photoionization[9] and that further each atomic electron may be described as moving in a screened Coulomb field both before and after ionization takes place. Photoionization is thus described as a single-electron process and photo-ionization cross sections for an electron in any subshell of an atom may be obtained by simple scaling procedures[10] from the photo-ionization cross sections for hydrogen which may be calculated exactly.[11]

* Postdoctoral Research Associate of the National Academy of Science–National Research Council.

[1] A. P. Lukirskii and T. M. Zimkina, Izv. Akad. Nauk SSSR, Ser. Fiz. **27**, 817 (1963) [English transl.: Bull. Acad. Sci. USSR, Phys. Ser. **27**, 808 (1963)].

[2] D. L. Ederer, Phys. Rev. Letters **13**, 760 (1964).

[3] P. Jaegle and G. Missoni, Compt. Rend. **252B**, 71 (1966).

[4] J. W. Cooper, Phys. Rev. Letters **13**, 762 (1964).

[5] E. J. McGuire, Ph.D. thesis, Cornell University, Ithaca, N. Y., 1965 (unpublished).

[6] F. Combet Farnoux and Y. Heno, Compt. Rend. **264B**, 138 (1967).

[7] L. G. Parrett, Rev. Mod. Phys. **31**, 616 (1959).

[8] L. V. Azaroff, Rev. Mod. Phys. **35**, 1012 (1963).

[9] Compton scattering and pair production will, of course, contribute to the absorption at high enough energies. In the energy range considered in this paper such processes have negligible effects and we shall assume that photoabsorption and atomic photo-ionization are equivalent processes. We also note that relativistic and retardation effects are unimportant in this energy range.

[10] J. C. Slater, Phys. Rev. **36**, 57 (1930).

[11] H. Hall, Rev. Mod. Phys. **8**, 358 (1936).

This simple hydrogenlike model is expected to break down in the soft x-ray range for two separate reasons. First, and most important, it assumes that electrons in the various subshells of an atom can be adequately described as moving in a screened Coulomb field. This assumption is expected to be valid only for innermost subshells and at photon energies large compared to the binding energy of a single electron in the subshell. These conditions are not fulfilled in the soft x-ray range, particularly for moderately heavy elements where M, N, and O subshells make substantial contributions to the total photo-ionization cross section. Second, recent experiments[12] have indicated that two-electron processes make a measurable contribution to the total absorption. A detailed theoretical treatment of such processes, which implies that electron-electron correlation be explicitly considered, has not yet been given and the extent to which they affect the spectral shape of measured absorption cross sections remains uncertain.

A logical first step towards a better understanding of the behavior of photoabsorption cross sections in the soft x-ray region is to calculate photo-ionization cross sections within the framework of a single-electron model but using a more appropriate central field. The few calculations that have been performed[4–6] indicate that such a model probably is capable of predicting the gross spectral shape of photo-ionization cross sections in the soft x-ray range.[13] However, effects of electron-electron correlation, which are specifically neglected in this model, are expected to have an appreciable effect on the spectral shape, particularly near absorption edges where an electron has barely enough energy to escape from the atom and thus its motion cannot be adequately described by a local central field. Thus the use of a better central field is expected to provide realistic photo-ionization cross sections only insofar as electron-electron correlation can be neglected.

The purpose of this paper is to investigate the behavior of atomic photo-ionization cross sections in the soft x-ray range by performing calculations for a number of atomic subshells for elements strategically located within the periodic table using a central-field model. The emphasis in this study is on the systematic trend of photo-ionization cross sections as a function of both atomic number and energy. This choice in emphasis is dictated by the expectation that, while atomic photo-ionization in the soft x-ray range occurs by and large subshell by subshell, the spectral shape of a given subshell contribution to the total photo-ionization cross section will depend critically on the position of the atom in the periodic table.

The central fields used in these calculations are those of Herman and Skillman[14] who have tabulated both the effective central field for each atom and the bound-state orbitals for each subshell. Calculation of photo-ionization cross sections using this atomic model is a straightforward procedure which could in principle be performed for any subshell of any atom using well-known numerical procedures.[15] We note in passing that the work of Herman and Skillman represents a considerable improvement over previous atomic models used for studying the Z dependence of atomic properties such as, e.g., the Thomas-Fermi model. However, the Herman-Skillman model has not been used extensively for this purpose. Work along these lines, as well as extensive study of the free-wave solutions of electrons moving in realistic atomic fields would, it appears, be extremely valuable. The properties of the Herman-Skillman model will be treated here insofar as they relate to the photo-ionization process and, it is hoped, may stimulate further work along the above lines.

In a sense, this paper represents a continuation of the work of Ref. 15, which was concerned only with outer subshell photo-ionization. In Sec. II the method of calculation is presented along with some discussion of the properties of the radial matrix elements which determine the cross section. In order to see how useful our model is for predicting cross sections, calculations for three elements (Al, Au, and Xe) were performed in energy ranges where detailed experimental cross sections are available. These results and comparisons with experimental data are given in Sec. III. Section IV presents detailed results for the $M_{\mathrm{II,III}}(3p)$ and $M_{\mathrm{IV,V}}$ $(3d)$ subshells. The photoionization cross sections for these subshells have been calculated for $Z=18$, 29, 32, 36, 45, 54, 63, 79, and 100 for $3p$, and for $Z=36$, 45, 54, 63, 79, and 100 for $3d$. The combined energy and Z dependence of these cross sections and its interpretation are the major results of this paper. In addition, calculations have been performed for subshells containing $3s$, $4s$, $5s$, $4p$, $4d$, $5p$, $5d$, and $4f$ electrons for certain elements. These results, while not providing information on the Z dependence of these contributions, provide an estimate of the energy dependence of photo-ionization from such subshells and are discussed in Sec. V. Section VI gives a discussion of all results and concluding remarks.

Quite recently a study using essentially the same model as ours has been made by Combet-Farnoux.[16] This work complements ours since Combet-Farnoux stresses in her calculations those subshells which make large contributions to photo-ionization cross sections in the soft x-ray range. Consequently, her work provides information on outer subshells ($4f$, $5p$, $5d$) of heavier elements whereas our work is concerned chiefly with the Z dependence of $3p$ and $3d$ subshells.

[12] T. A. Carlson and M. O. Krause, Phys. Rev. Letters **17**, 1079 (1966), and references quoted therein.
[13] U. Fano, Science **153**, 522 (1966).
[14] F. Herman and S. Skillman, *Atomic Structure Calculations* (Prentice-Hall Inc., Englewood Cliffs, N. J., 1963).
[15] J. W. Cooper, Phys. Rev. **128**, 681 (1962).
[16] F. Combet Farnoux, Compt. Rend. **264B**, 1728 (1967).

II. METHOD OF CALCULATION

If all of the electrons in a given subshell are assumed to move in the same central field, the cross section for photo-ionization from the nlth subshell may be written as[17]

$$\sigma_{nl}(\epsilon)=\frac{4\pi\alpha a_0^2}{2}\frac{N_{nl}(\epsilon-\epsilon_{nl})}{2l+1}[lR_{\epsilon,l-1}^2+(l+1)R_{\epsilon,l+1}^2]. \quad (1)$$

Here ϵ_{nl} (in rydbergs) is the binding energy for an electron in the nlth subshell, α is the fine-structure constant (1/137), N_{nl} ls the number of electrons in the subshell, and ϵ (in rydbergs) is the energy of the ionized electron, i.e., $h\nu=\epsilon-\epsilon_{nl}$, where $h\nu$ is the energy of the incident photon. The radial matrix elements are

$$R_{\epsilon,l\pm1}=\int_0^\infty P_{nl}(r)rP_{\epsilon,l\pm1}(r)dr, \quad (2)$$

where $P_{nl}(r)$ and $P_{\epsilon,l\pm1}(r)$ are solutions of the radial Schrödinger equation

$$\left(\frac{d^2}{dr^2}+V(r)+E-\frac{l(l+1)}{r^2}\right)P_{El}(r)=0: \quad E=\epsilon,\ \epsilon_{nl}$$
$$V(r)\underset{r\to0}{\longrightarrow}\frac{2Z}{r}: \quad V(r)\underset{r\to\infty}{\longrightarrow}\frac{2}{r}. \quad (3)$$

Here r is in units of $a_0(=5.29\times10^{-9}$ cm) and the radial wave functions P_{nl} and $P_{\epsilon l}$ satisfy the normalization conditions

$$\int_0^\infty P_{nl}^2(r)dr=1 \quad (4)$$

$$P_{\epsilon l}\lim_{r\to\infty}(r)=\epsilon^{-1/4}\sin[\epsilon^{1/2}r-\tfrac{1}{2}l\pi-\epsilon^{-1/2}\ln2\epsilon^{1/2}r+\delta_l(\epsilon)], \quad (5)$$

where $\delta_l(\epsilon)$ is the phase shift. This normalization of $P_{\epsilon l}(r)$ is the usual normalization of continuum wave functions per unit energy range.

Equations (1–5) are the same as Eqs. (4–8) of Ref. 15 except that here the same central potential $V(r)$ is used for all radial wave functions, bound or free, which satisfy Eq. (3) with the normalization conditions (4) and (5). The potentials $V(r)$ are given in Ref. 14 as well as the normalized radial bound-state orbitals $P_{nl}(r)$ and the binding energies ϵ_{nl}. The photo-ionization cross sections for any subshell at any energy ϵ may be obtained using Eqs. (1–5). This involves solving Eq. (3) for $l'=l\pm1$ numerically, obtaining the radial matrix elements $R_{\epsilon,l\pm1}$ by numerical integration, and evaluating the cross section using Eq. (1). The numerical procedures used here are the same as in Ref. 15.

Before proceeding to a discussion of numerical results, it will be useful to discuss some of the properties of the central-field model outlined above.

[17] Equation (1) is equivalent to Eq. (7) of Ref. 15 with the added restriction that it applies only to complete subshells.

As was pointed out in Ref. 15, the photo-ionization cross section for a particular subshell can be considered as part of the total oscillator strength spectral distribution defined as

$$\frac{df}{d\epsilon}=\frac{df_{l+1}}{d\epsilon}+\frac{df_{l-1}}{d\epsilon}=\tfrac{1}{3}N_{nl}(\epsilon-\epsilon_{nl})\times[lR_{\epsilon,l-1}^2+(l+1)R_{\epsilon,l+1}^2], \quad (6)$$

where ϵ now refers to both discrete and continuum final states. The total oscillator strength for all transitions from a given subshell is

$$\int\frac{df}{d\epsilon}d\epsilon=N_l \quad (7)$$

by Eqs. (15) and (16) of Ref. 15, and therefore the total oscillator strength for all subshells is $\sum N_l=Z$; i.e., the oscillator strengths in a central-field model obey the Thomas-Kuhn sum rule as well as the more specific rule implied by (7) which states that the sum of all oscillator strengths for dipole allowed transitions in a particular subshell must equal the total number of electrons in the subshell. While the Thomas-Kuhn rule is rigorously valid for all dipole transitions[18] from the ground state of an atom, it does not apply subshell by subshell as is implied by Eq. (7) since transitions to filled subshells will be excluded by the Pauli principle. However, use of the same effective central field for all electrons compensates for this since the sum of all Pauli-forbidden transitions is then zero. For example, if the total oscillator strength distribution of Ne ($1s^22s^22p^6$) is calculated in the central-field approximation, the oscillator strengths of the "upward" transitions $1s\to2p$ and $2s\to2p$ for the K and L_I subshells will exactly cancel the "downward" transitions $2p\to2s$ and $2p\to1s$ since the same one-electron wave function and binding energies are used in both calculations. These considerations become important, as we shall see in Sec. IV, when the Z dependence of the photo-ionization cross section for a particular subshell is considered, since a new subshell (nl) becoming occupied with increasing Z corresponds to a reduction in photo-ionization cross section for inner subshells whose orbital angular momentum quantum number is $l'=l\pm1$ within the framework of our model.

The cross sections given by Eq. (1) can be considered as composed of two parts, namely,

$$\sigma_{nl}{}^+=\frac{4\pi\alpha a_0^2(\epsilon-\epsilon_{nl})}{3}\frac{N_{nl}}{2l+1}(l+1)R_{\epsilon,l+1}^2 \quad (8)$$

and

$$\sigma_{nl}{}^-=\frac{4\pi\alpha a_0^2(\epsilon-\epsilon_{nl})}{3}\frac{N_{nl}}{2l+1}lR_{\epsilon,l-1}^2. \quad (9)$$

[18] H. A. Bethe and E. E. Salpeter, *Quantum Mechanics of One and Two Electron Atoms* (Academic Press Inc., New York, 1957), p. 260.

Thus the energy dependence of the cross sections, apart from the factor $\epsilon-\epsilon_{nl}$, depends on the energy dependence of the matrix elements is given by Eq. (2).

It is convenient to factor this energy dependence into two independent parts. Consider a free-wave solution $\bar{P}_{\epsilon l}$ of Eq. (3) normalized so that $\bar{P}_{\epsilon l}=r^{l+1}$ near the origin. Actually, the numerical solution of Eq. (3) is started at the origin with this normalization so that the process of solving Eq. (3) consists of numerically integrating Eq. (3) outwards to the point where the potential $V(r)$ reaches its asymptotic value $2/r$ and then normalizing the solution so that it satisfies Eq. (5). This is accomplished by determining a constant $C_l(\epsilon)$ as outlined in Appendix A of Ref. 15[19] so that the normalized solution satisfying Eq. (5) is

$$P_{\epsilon l}(r)=C_l(\epsilon)\bar{P}_{\epsilon l}(r). \tag{10}$$

The energy dependence of the matrix element may then be factored into two parts, i.e.,

$$R_{\epsilon,l\pm1}=C_{l\pm1}(\epsilon)\bar{R}_{\epsilon,l\pm1}, \tag{11}$$

where $\bar{R}_{\epsilon,l\pm1}$ represents the matrix element of Eq. (2) with $P_{\epsilon,l\pm1}(r)$ replaced by $\bar{P}_{\epsilon,l\pm1}(r)$. For subshells which lie close to the nucleus, $\bar{R}_{\epsilon,l\pm1}$ is almost constant over a wide range of energies since the potential $V(r)$ is large in that region. Consequently, we expect the energy dependence of the partial photo-ionization cross sections given by Eqs. (8) and (9) to be almost completely determined by the normalization factor $C_{l\pm1}(\epsilon)$ near thresholds. Note that the normalization constant $C_{l\pm1}(\epsilon)$ depends upon the behavior of the potential $V(r)$ over its entire range and that consequently the spectral shape of the cross section by an interior subshell may be almost completely determined by the behavior of the potential outside the subshell.

For subshells lying rather far out, the unnormalized matrix element $\bar{R}_{\epsilon,l\pm1}$ will vary with energy. Its value is determined by the overlap of the wave function P_{nl} and $\bar{P}_{\epsilon,l\pm1}$ in the integrand of Eq. (2). The spectral behavior of $\bar{R}_{\epsilon,l\pm1}$ will in general depend on whether or not the nl subshell radial wave function is nodeless $(l=n-1)$,[20] and on the strength of the potential $V(r)$.

The spectral shape of the partial cross sections corresponding to variations in $\bar{R}_{\epsilon,l\pm1}$ will be different for different value of n. However, variations of $C_{l\pm1}(\epsilon)$ will produce the same variation in cross sections for all subshells having the same value of l.

The normalization constant $C_l(\epsilon)$ is equivalent to the "enhancement factor" used in similar treatments in nuclear physics[21] and is obviously related to the phase shift defined by Eq. (5). While for certain simple analytic potentials the relationship between $\delta_l(\epsilon)$ and $C_l(\epsilon)$ can be established,[22] for potentials of Coulomb form an exact relationship has not been given. The work of Seaton[23] suggests that C behaves as

$$C_l(\epsilon)=\frac{1}{|A_l(\epsilon)\cos\delta_l(\epsilon)+G_l(\epsilon)\sin\delta_l(\epsilon)|}, \tag{12}$$

which indicates that $C_l(\epsilon)$ may vary rapidly when $\delta_l(\epsilon)$ does, the exact variation depending upon the energy-dependent factors $A_l(\epsilon)$ and $G_l(\epsilon)$. Comparisons of $C_l(\epsilon)$ and $\delta_l(\epsilon)$ for a particular case will be given later.

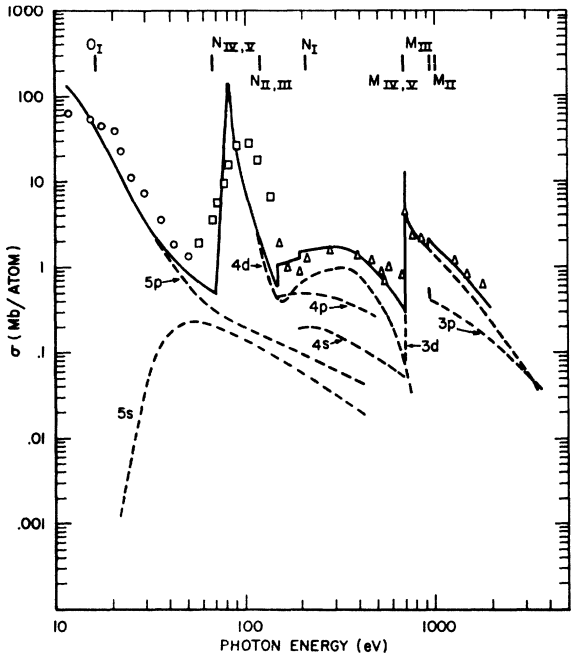

FIG. 1. Photo-ionization cross section in xenon. The dashed lines are the calculated contributions of the individual subshells; the solid line is the total calculated cross section. The circles are the experimental data of Samson (Ref. 23), the squares those of Ederer (Ref. 2), and the triangles the results of Lukirskii *et al.* (Ref. 24).

III. COMPARISON WITH EXPERIMENT

For Xe, the absorption cross section has been measured from threshold to ~2 keV.[2,24,25] In Fig. 1 measured cross sections are compared with calculated cross sections for the M, N, and O shells.[26] This figure shows that

[19] Equations (A4) and (A5) of Ref. 15 are incorrect. They should read:

$$x^2=A(r)+x^{1/2}d^2(x^{-1/2})/dr^2 \tag{A4}$$

$$x^2\cong A-A^{-1}A''/4+(5/16)(A')^2A^{-2}. \tag{A5}$$

[20] U. Fano, in *Proceedings of the Second International Conference on the Physics of Electronic and Atomic Collisions* (W. A. Benjamin Inc., New York, 1961), p. 10. The tentative generalizations of the behavior of various subshell contributions implied in this work are considerably modified by the detailed calculations reported in the present paper.

[21] M. L. Goldberger and K. M. Watson, *Collision Theory* (John Wiley & Sons, Inc., New York, 1964), p. 274.

[22] R. Jost and W. Kohn, Phys. Rev. **87**, 977 (1952).

[23] M. J. Seaton, Monthly Notices Roy. Astron. Soc. **118**, 504 (1958).

[24] J. A. R. Samson, J. Opt. Soc. Am. **54**, 842 (1964).

[25] A. P. Lukirskii, I. A. Brytov, and T. M. Zimkina, Opt. i Spektroskopiya **17**, 438 (1964) [English transl. Opt. Spectry. (USSR) **17**, 234 (1964)].

[26] The M_I contribution is not included in Fig. 1.

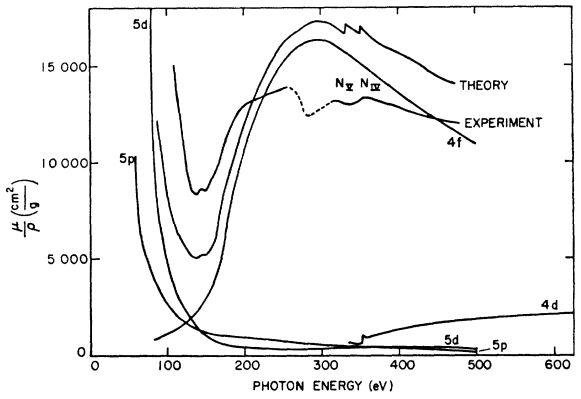

FIG. 2. Photo-ionization cross section in gold. The experimental curve is due to Jaegle and Missoni (Ref. 3). The $4f$ partial cross section has been shifted 24 eV to the left as discussed in Sec. II.

in addition to providing a breakdown of the various subshell contributions the calculations correctly predict the spectral shape over a broad spectral range. The curves also indicate the breakdown of the hydrogenic approximation.[27] In the energy range under consideration the hydrogenic model gives a completely different spectral shape for the total cross section from that observed. In particular, it fails to predict the prominent peak in the cross section at about 90 eV and the broad secondary maximum between 200 and 500 eV. The central-field model does show these features and furthermore indicates that both maxima are primarily due to electrons ejected from the $N_{IV,V}(4d)$ subshell, i.e., that the partial cross section for this subshell is bimodal.

The limitations of the central-field model are also clearly brought out in Fig. 1. In particular the peaks at threshold and in the neighborhood of the $N_{IV,V}$ and $M_{IV,V}$ thresholds are overestimated by the calculation. These are just the regions which, in a central-potential model, correspond to low velocity of the outgoing electron and the electron-electron correlation effects mentioned in Sec. I are expected to be most important. As discussed in Ref. 15, these effects are expected to "smear out" the sharp features in calculations based on the central-field model. In spite of these defects the total oscillator strength over the energy range from threshold to 2 keV is approximately the same for both calculation (36.9) and experiment (37.3). Figure 1 also indicates that the peaking of the cross section above the $N_{IV,V}$ threshold is accompanied by a similar peaking above the $M_{IV,V}$ threshold. In fact the measured value right above the $M_{IV,V}$ threshold (while based on one experimental point) appears to be quite large (~4.3 mb). Recent experimental[28] work has indicated that the cross section in this energy range does peak above threshold in much the same manner and over essentially the same range of energies as above the $N_{IV,V}$ threshold. The calculations indicate and, in fact, overestimate this behavior.

Figure 2 shows results for the N and O shells of gold[29] together with the experimental results of Jaegle and Missoni.[3] The dashed-line part of the latter data indicates a region of experimental uncertainty. The agreement between theory and experiment is quite good throughout, even to reproducing the shape of the minimum at ~145 eV which comes about from the summed contributions of the $O_{II,III}$, $O_{IV,V}$ and $N_{VI,VII}$ subshells. Here two adjustments were made in the calculated cross sections for purposes of comparison with experiment: the $N_{VI,VII}$ cross section which was calculated using the *theoretical* threshold energy, was uniformly translated so that its threshold is at the *experimental* value. Further, the spin-orbit splitting of the $N_{IV,V}$ subshell into $4d_{3/2}$ and $4d_{5/2}$ (N_{IV} and N_V) components has been introduced by weighing the total cross section for this subshell by 0.6 and 0.4 and shifting the individual contributions to the experimental thresholds as above.

These adjustments are made to give an example of how realistic central-field calculations can be used as an aid to interpreting experimental results. The correction for spin-orbit splitting is done exactly in the same manner as in hydrogenic calculations and assumes that the radial matrix elements [Eq. (2)] are insensitive to the energy splitting. The shifting of the $N_{VI,VII}$ contribution is based on the same argument and is made here because of the large difference between the experimental binding energy[30] (85 eV) and the binding energy obtained from Ref. 14 (109 eV) for the $4f$ subshell. A calculation similar to ours made without this adjustment (Ref. 6) produces essentially the same spectral shapes but with a much deeper minimum in the total cross section. The large difference between experimental and theoretical binding energies for the $4f$ subshell indicates that the $4f$ radial wave function used in the computation is probably too compact. A more diffuse radial wave function would tend to flatten out the $M_{VI,VII}$ cross section and result in even better agreement between calculation and experiment. The

TABLE I. Photo-ionization cross section of aluminum in mb/atom.

Photon energy (keV)	Experiment[a]	Hydrogenic	Rakavy and Ron[b]	This paper
5	8560	8150	8375	8578
10	1150	1060	1103	1139
15	337.2	316		332.6
20	137.9	131		138.0
30	37.78	36.8	37.47	38.48

[a] Reference 31. [b] Reference 32.

[27] Hydrogenic calculations (not shown in Fig. 1) may be easily computed using the data compiled by M. Lewis, National Bureau of Standards Report No. 2457, 1953 (unpublished).

[28] R. Deslattes (to be published).

[29] Substantially the same curve has been calculated by the same method by F. Combet Farnoux and Y. Heno in Ref. 6. We wish to thank these authors for communicating these results prior to publication.

[30] J. A. Bearden and A. F. Burr, Rev. Mod. Phys. **39**, 125 (1967).

results obtained both here and in Ref. 6 indicate that solid-state effects are not important for gold in the energy range considered.

As a final example we have calculated the K- and L-shell cross sections in Al from 5–30 keV. (The M-shell contribution in this energy range is negligible.) The results are shown in Table I along with a hydrogenic calculation,[27] experimental results,[31] and the calculation of Ron[32] who used a modified Thomas-Fermi potential. From this table it is clear that both Ron's calculation and our results agree quite well with experiment,[33] while the hydrogenic cross sections are consistently low.

This last result is to be expected. At high energies (in the MeV range) effective screening should be neglected since photoabsorption takes place primarily near the nucleus.[34,35] The use of screened wave functions within the hydrogenic approximation [which at high energies is proportional to $(Z-S)^5$, where S is the effective screening constant] as in Table I is thus expected to underestimate photoabsorption at high energies. For low-Z materials it has long been known[35] that the screened hydrogenic approximation also underestimates the cross section at lower energies (i.e., in the range 10–100 keV). The calculations of Ron and this paper, which account for screening effects realistically, have the correct high-energy behavior, hence the improved agreement between these calculations and experiment.

These examples indicate that moderately good agreement between experiment and calculations based on our model is obtained provided the cross sections that we compute are not rapidly varying—and that the agreement will be better at higher energies. They also show that the gross spectral shape of cross sections is correctly predicted, so that our calculations are expected to indicate in what energy ranges maxima and minima will occur. In the next section we explore the matter further by studying in detail the behavior of $M_{\mathrm{II,III}}$ and $M_{\mathrm{IV,V}}$ subshells as a function of both energy and Z.

IV. PHOTO-IONIZATION OF $3p$ ($M_{\mathrm{II,III}}$) AND $3d$ ($M_{\mathrm{IV,V}}$) SUBSHELLS

A. Effective Central Potential

The Z dependence of the partial cross sections given by Eqs. (8) and (9) of Sec. II can be understood by considering the effective potential $\Phi_l(r)=-V(r)+[l(l+1)/r^2]$ indicated in Eq. (3). Curves of this potential appropriate to the final states in $nd\rightarrow\epsilon f(l=3)$ transitions are shown in Fig. 3. Except for Kr these

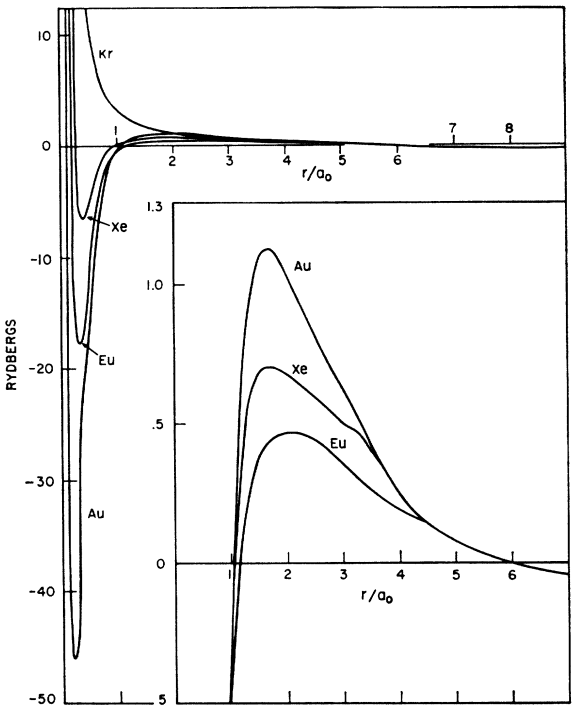

FIG. 3. The potential curves for $l=3$ electrons in Kr, Xe, Eu, and Au.

curves have the form of a "potential well" inside the atom, a small repulsive barrier (shown in the inset) and finally a broad well which is the same for all cases in the region where $V(r)$ has reached its asymptotic form $2/r$. The appearance of an "inner well" in the potential $\Phi_l(r)$ with increasing Z implies a radical change in the radial distribution of its eigenfunctions. In first approximation the discrete eigenfunctions of $\Phi_l(r)$ may be classified into two groups: eigenfunctions of the "inner well" corresponding to bound states in the atomic ground state for given l, and bound states of the outer well corresponding to the Rydberg series of excited states. This concept was used long ago[36] to explain the properties of the rare earths. According to this picture the formation of the $4f$ subshell is considered as a transfer of discrete eigenfunctions from the "outer" to the "inner well" with a consequent marked reduction in average radius of the $4f$ radial wavefunction. While for $l<3$ the effective potential generally does not have a positive "barrier" as shown in Fig. 3, nevertheless the effective potential for large Z will have "inner" and "outer" valleys since $V(r)$ is the same for all l. The formation of new subshells may thus be considered as a less drastic "moving in" of a particular nl radial eigenfunction with increasing Z with a consequent increase in binding energy.

The energy dependence of continuum eigenfunctions of potentials such as those shown in Fig. 3 and con-

[31] J. H. Hubbell and M. J. Berger, National Bureau of Standards Report No. 8681, 1966 (unpublished).
[32] A. Ron, Ph.D. thesis, University of Jerusalem, Jerusalem, Israel, 1965 (unpublished). We wish to thank Dr. Ron for making these results available to us.
[33] The experimental results shown here are those obtained in Ref. 30 by correcting the best experimental values for the effects of pair production and Compton scattering.
[34] R. H. Pratt, Phys. Rev. **117**, 1017 (1960).
[35] G. W. Grodstein, Natl. Bur. Std. (U. S.), Circ. No. **583** (1959).
[36] M. G. Mayer, Phys. Rev. **60**, 184 (1941).

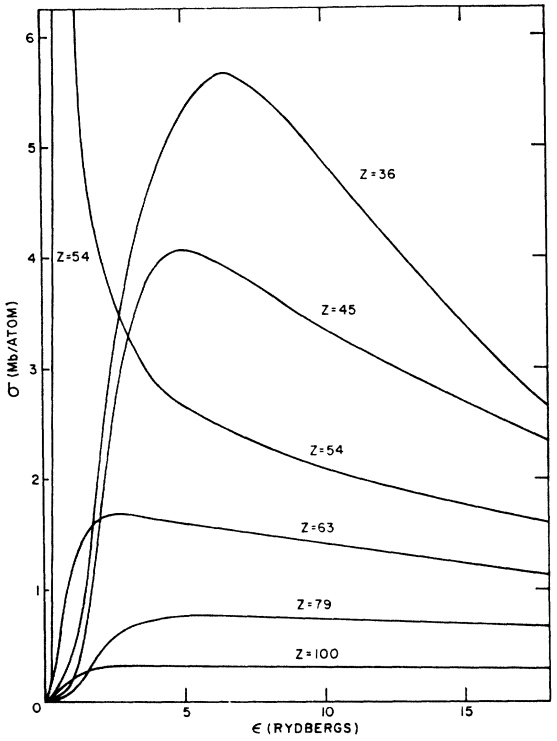

FIG. 4. The $3d \rightarrow \epsilon f$ partial cross sections for Kr, Rh, Xe, Eu, Au, and Fm. The maximum for $Z=54$ (Xe) is 13.6 Mb at $\epsilon=0.6$ Ry.

sequently the matrix elements of Eqs. (8) and (9) will depend on the strength of the "inner well" and on the details of the potential barrier. Typically, a zero-energy free-wave solution of Eq. (3) will contain as many antinodes in the inner region as there are occupied subshells of the atom corresponding to the value of l. With increasing energy, nodes of the free-wave solution will move to smaller value of r. For initial- and final-state radial wave functions which have nodes "inside the atom," the value of the matrix element and hence the cross section will depend on the relative position of these nodes at a particular energy.

B. 3d Subshell; $l \rightarrow l+1$ Transitions

The results of our calculations of the $3d \rightarrow \epsilon f$ transitions in Kr, Rh, Xe, Eu, Au, and Fm are plotted in Fig. 4. The outstanding feature of these results is the large deviation from monotonic decreasing behavior in the threshold region (outgoing electron energies up to $\sim$200 eV) even for Z as high as 100; the maximum occurs at various energies above threshold for the different Z's and, in each case, is orders of magnitude larger than the threshold value. To understand this, consider the behavior of the radial wave functions $P_{\epsilon f}(r)$ for krypton ($Z=36$). In Fig. 5 the $3d$ wave function is plotted along with the f wave for $\epsilon=0$ and 6 Ry. At threshold the ϵf radial function is kept far out by the centrifugal repulsion so that its overlap with the $3d$ is very small. This leads to a small dipole matrix element and, hence, a small cross section at threshold. With increasing energy the ϵf wave function penetrates deeper and deeper into the core, thus increasing the overlap and the cross section. The $\epsilon=6$ Ry ϵf wave function shows a larger overlap than at threshold and also a slight amount of cancellation since the ϵf wave function now has a node at $r\cong 2$. As the energy increases further, cancellation becomes increasingly important since the ϵf wave function continues to move in. The cross section as a function of energy thus reaches a maximum value and then starts to decrease, owing to this cancellation.

Going up in Z to rhodium ($Z=45$), the situation is substantially the same as in krypton. The maximum is, however, closer to threshold in rhodium; at 4.8 Ry above threshold as opposed to 6.5 Ry in krypton. The effective f wave potential for Xe ($Z=54$), as shown in Fig. 3, has a fairly deep well followed by a barrier about 0.7 Ry high. This barrier, although small, is broad enough to keep the ϵf wave function far out at threshold. When the ϵf wave function has an energy comparable with the barrier height it penetrates quite deeply giving a very rapid rise of the cross section with energy to its maximum at 0.6 Ry. With increasing energy, the cross section drops off rapidly as shown in Fig. 4. This large peak in the Xe cross section can also be described as a resonance lying close to threshold. The resonant character of the free-wave solution $P_{\epsilon f}(r)$ and its effect on the cross section can be seen by an analysis of the dipole matrix element $R_{\epsilon f}$ into components $C_f(\epsilon)$ and $\bar{R}_{\epsilon,f}$ as indicated by Eq. (11). The energy dependence of these factors as well as the phase shift $\delta_f(\epsilon)$ defined by Eq. (2) is shown in Table II. The increase of $\delta_f(\epsilon)$ by $\sim\pi$ between $\epsilon=0$ and $\epsilon=2$ indicates that $P_{\epsilon f}(r)$ has gone through a resonance or that, alternatively, the first node of this wave function has moved from outside to inside the atom. This change of phase shift is accompanied by a rapid variation of the "enhancement factor" $C_f(\epsilon)$ and

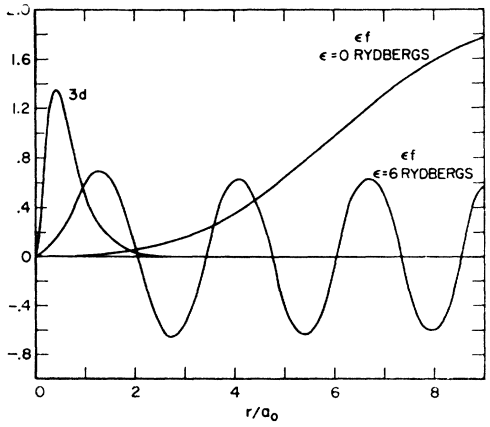

FIG. 5. The normalized $3d$ and ϵf wave function in Kr.

a relatively slow decrease of $\bar{R}_{\epsilon,f}$ due to a change in overlap between discrete and continuum wave functions. The table further shows that the decrease in cross section at higher energies is primarily due to a decrease in $\bar{R}_{3d\to\epsilon f}$, i.e., to the effect of overlap rather than to variations of $C_f(\epsilon)$.

In europium ($Z=63$), the maximum lies at 2.8 Ry and the cross section is much smaller than for Kr, Rh, or Xe. Integration of the total continuum oscillator strength ($df_{l+1}/d\epsilon$) of Eq. (6) yields ~9.6 for Eu and ~13.9 for Kr, Rh, and Xe.[37] This sharp decrease in integrated continuum oscillator strength is related to the filling of the $4f$ subshell which on the basis of the potentials of Ref. 14 starts at $Z=58$. Note that the large decrease of the $3d\to\epsilon f$ total continuum oscillator strength with increasing Z does not constitute a violation of the Thomas-Kuhn sum rule for the atom as a whole, but merely a transfer of oscillator strength from the $3d$ to the $4f$ subshell.

We interpret the change in spectral shape of the $3d\to\epsilon f$ cross section as a function of Z as follows. For $Z=36$, 45, and 54 the cross section peaks due to the resonance described above for Xe. With increasing Z, this resonance becomes narrower and moves closer to threshold owing to the increase in the potential $V(r)$. By $Z=63$, $V(r)$ is strong enough to bind $4f$ electrons inside the atom so that the resonance has disappeared into the discrete spectra and has in effect become the $4f$ eigenfunction.

In gold ($Z=79$), although the total continuum oscillator strength for $3d\to\epsilon f$ transition is the same as in Eu, the maximum lies at higher energy. This outward shift in energy of the maximum is due to an increase in the height of the barrier (shown in the inset of Fig. 3) between the two regions of negative effective central potential. The penetration of an f wave with increasing energy is delayed more in Au than in Eu by the larger barrier. Note that the Eu and Au effective potentials cross and that this crossing has a marked effect on the calculated cross sections. While the accuracy of the Herman-Skillman potentials may be poor for values r in the regions where crossings occur, the implications of such crossings seem to merit further investigation.

TABLE II. Normalization factor $C_f(\epsilon)$, phase shift $\delta_f(\epsilon)$, and unnormalized matrix element $\bar{R}_{3d\to\epsilon f}$ in xenon.

Energy (Ry above threshold)	$\delta_f(\epsilon)$	$C_f(\epsilon)$	$10^3\,\bar{R}_{3d\to\epsilon f}$
0	0.14	53.2	0.150
0.25	1.0	246	0.148
0.6	2.2	1530	0.145
1	2.8	1310	0.142
1.3	3.1	1040	0.140
2	3.3	908	0.135
4	3.5	818	0.123

[37] These values were obtained by graphically integrating our curves from threshold to 1000 Ry and using an asymptotic representation for energies above 1000 Ry.

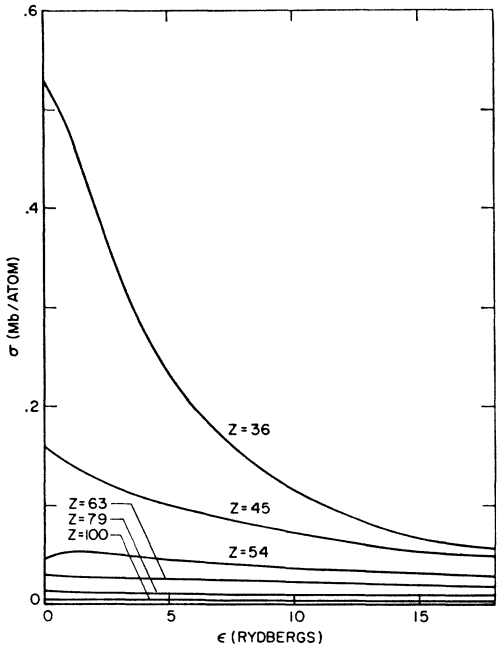

FIG. 6. The $3d\to\epsilon p$ partial cross sections for Kr, Rh, Xe, Eu, Au, and Fm.

Finally, in fermium ($F=100$), the total continuum oscillator strength of $3d\to\epsilon f$ transitions has decreased from the value of ~9.3 for gold to ~6.4 since the effective potential is strong enough to bind $5f$ electrons inside the atom. Although we have made no calculations for values of Z between 79 and 100, we expect that the spectral shape of the cross sections will follow a pattern similar to that between $Z=45$ and 63, i.e., that the maximum at $Z=79$ will move toward threshold, peak, and disappear with increasing Z as the $5f$ subshell fills.

C. 3d Subshell; $l\to l-1$ Transitions

The $3d\to\epsilon p$ cross sections are shown in Fig. 6. These cross sections are typically an order of magnitude smaller than the $3d\to\epsilon f$ cross sections for a given Z and consequently make little contribution to the total cross sections.

The general trend of these cross sections is to become smaller and flatter with increasing Z. The shape of the cross sections is determined in detail by the position of the first two nodes of the final-state ϵp wave functions which overlap the $3d$ wave function in all cases. Without going into details, we note that increasing the potential strength in going from $Z=36$ to $Z=45$ has a greater effect on the spectral shape of the cross section than in going from $Z=45$ to $Z=63$ even though the $5p$ subshell is filled between $Z=45$ and $Z=63$. Consequently, we expect that the spectral shape of these cross sections will depend more on the unnormalized matrix element $\bar{R}_{\epsilon,p}$ than on the normalization factor $C_p(\epsilon)$ for these transitions.

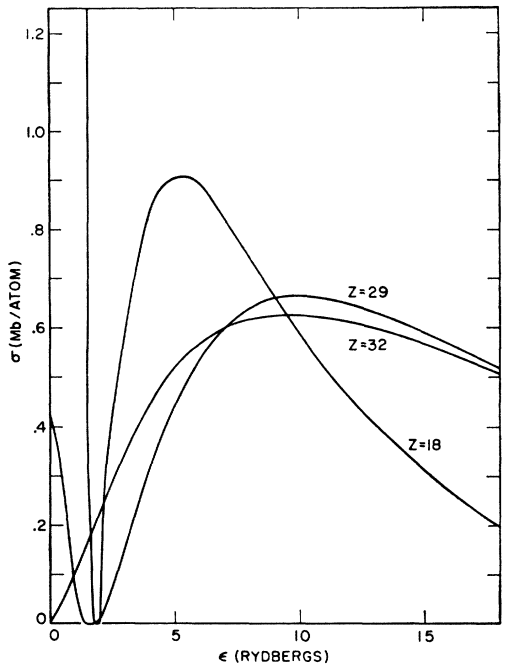

FIG. 7. The $3p \rightarrow \epsilon d$ partial cross sections for Ar, Cu, and Ge. The $Z=18$ (Ar) curve reaches a maximum of 51 mb at threshold.

D. 3p Subshell; $l \rightarrow l+1$ Transitions

Previous work[38] has shown that the $3p \rightarrow \epsilon d$ partial cross section of Ar vanishes at about 2 Ry above threshold since the matrix element in Eq. (2) changes sign. In Fig. 7, the $3p \rightarrow \epsilon d$ cross section is shown for Ar ($Z=18$), Cu ($Z=29$), and Ge ($Z=32$). The curves show that with increasing potential strength the zero of the partial cross section moves closer to the threshold. However, the partial cross section for Cu still vanishes above threshold even though the effective potential is strong enough to fill the $3d$ subshell. This result, coupled with the fact that the binding energies of a $3d$ electron in Cu is much less than the neighboring elements[39] (Ni and Zn) indicates that the spectral shape of the $3p \rightarrow \epsilon d$ cross sections for neighboring elements may be quite different than the curves shown here and that no general rule of the Z dependence of these cross sections can be given. A detailed investigation would require further calculations and analysis of the cross sections in terms of the effective central potential as was done for $3d \rightarrow \epsilon f$ transitions. The $3p \rightarrow \epsilon d$ partial cross sections for Kr, Rh, Xe, Eu, Au, and Fm

[38] The work of Ref. 15 on Ar used a different potential than was used here and detailed calculations were not made in the region of the second maximum. Consequently, the $3p^6$ subshell cross section reported in Fig. 1 of Ref. 4 is only a crude estimate. The total cross section for Ar using the Herman-Skillman potential has been calculated and is in closer agreement with the experimental results than the work of Ref. 4 in the 50–120 eV range. These calculations will be reported in a future publication.

[39] From Ref. 14 the binding energies of a $3d$ electron in Ni, Cu, and Zn are 1.115, 0.743 and 1.258 Ry, respectively.

TABLE III. Normalization factor $C_d(\epsilon)$ and unnormalized matrix element $\bar{R}_{3p\rightarrow\epsilon d}$ in Kr and Rh.

	Krypton ($Z=36$)		Rhodium ($Z=45$)	
ϵ(Ry)	$C_d(\epsilon)$	$10^3\,\bar{R}_{3p\rightarrow\epsilon d}$	$C_d(\epsilon)$	$10^3\,\bar{R}_{3p\rightarrow\epsilon d}$
0	210	0.272	415	0.106
5	342	0.278	505	0.105
1	326	0.284	595	0.104
2	308	0.289	625	0.102
4	318	0.288	623	0.098
8	326	0.265	630	0.089

($F=36$, 45, 54, 63, 79, and 100) are shown in Fig. 8. The Z dependence of these cross sections can be described by the resonance schematization used previously for $3d \rightarrow \epsilon f$ transitions. We interpret the first maximum in Kr as a "$4d$" resonance and the first maxima in Rh, Xe, and Eu as "$5d$" resonances. The "enhancement factor" $C_d(\epsilon)$ and reduced matrix elements $\bar{R}_{3p\rightarrow\epsilon d}(\epsilon)$ for Kr and Rh shown in Table III indicate that the first maximum in these cross sections is due almost entirely to an increase of $C_d(\epsilon)$ near threshold and that the gradual decrease of the cross section at higher energies comes about from the decrease of the reduced matrix element $\bar{R}_{3p\rightarrow\epsilon d}(\epsilon)$. Note that the second broad peak in the Kr cross section is also due primarily to the variation of $C_d(\epsilon)$ and from this standpoint may be considered as a second or "$5d$" resonance. Thus the single peak in Rh corresponds to the second peak in Kr, the first peak having disappeared as a result of the $4d$ subshell having been partially filled with a resulting decrease of the $3p \rightarrow \epsilon d$ total continuum oscillator strength. For Xe the "$5d$" resonance is a sharp peak near threshold which in turn disappears when the $5d$ subshell fills. The change in cross section between Xe and Eu indicates that while the effective potential has not increased in strength enough to bind a $5d$ electron in the Eu atom, a considerable portion of the continuum oscillator strength has been transferred to the allowed $3p \rightarrow 5d$ transition, i.e., that the $5d$ radial wave function becomes gradually more compact with increasing potential strength in contrast to the rapid decrease in the average radius of

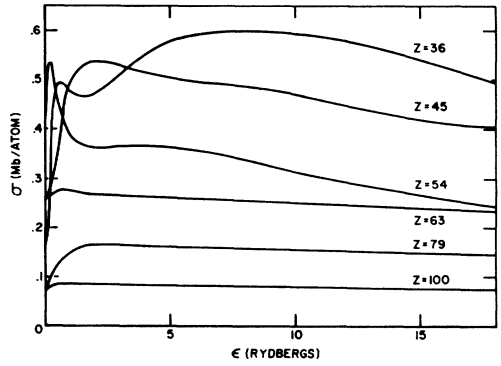

FIG. 8. The $3p \rightarrow \epsilon d$ partial cross sections for Kr, Rh, Xe, Eu, Au, and Fm.

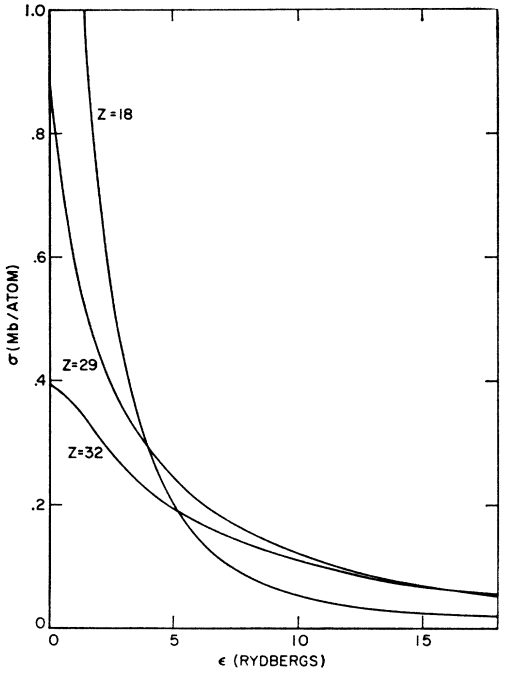

FIG. 9. The $3p \rightarrow \epsilon s$ partial cross sections for Ar, Cu, and Ge. The $Z=18$ (Ar) curve reaches a maximum of 3.8 mb at threshold.

the $4f$ electron discussed previously. Between Eu and Au and between Au and Fm, the cross section becomes smaller because of filling of the $5d$ subshell and binding of a single electron in the $6d$ subshell in Fm.

E. $3p$ Subshell; $l \rightarrow l-1$ Transitions

Cross sections for $3p \rightarrow \epsilon s$ transitions for the same elements as in the previous section are presented in Figs. 9 and 10. Typically, these cross sections tend to be largest at threshold (since there is no centrifugal barrier in this case) and to become smaller and flatter with increasing Z. While an interpretation of the relative maxima in these curves in terms of the binding of ns electrons with increasing Z could be made, the small values of these cross sections relative to the $3p \rightarrow \epsilon d$ contributions make such an analysis of academic interest. However, the relative values at threshold of the two partial cross sections may be of some help in interpreting the structure in the vicinity of absorption edges since it provides an indication of the relative strengths of $3p \rightarrow nd$ and $3p \rightarrow ns$ transitions. The same considerations, of course, apply to the relative strengths at threshold of the $3d \rightarrow \epsilon p$ and $3d \rightarrow \epsilon f$ cross sections of Figs. 4 and 6.

F. High-Energy Behavior and Deviations from the Hydrogenic Approximation for $3d \rightarrow \varepsilon f$ and $3p \rightarrow \varepsilon d$ Transitions

The results presented in Figs. 4, 6, 7, and 8 have been plotted on a linear scale in order to emphasize the difference in threshold behavior for different values of Z and to explore the systematics of this behavior. Consequently, the flattening of these curves with increasing Z above, say, 10 Ry is not surprising since only a small fraction of the binding energy is represented by these curves for large Z. The hydrogenic approximation plotted on the same scale would show substantially the same effect.

In order to present a clearer picture of the decrease of cross sections at high energies we have plotted the data for $3d \rightarrow \epsilon f$ and $3p \rightarrow \epsilon d$ transitions for Kr, Xe, and Au on a double logarithmic scale versus photon energy and extended the calculations for these transitions above threshold to 1000 Ry. These results are shown in Figs. 11 and 12 along with calculations based on the hydrogenic approximation[11] with Slater screening.[10] These curves show in what spectral ranges the threshold effects described in detail in the previous sections are important. They also show that the hydrogenic results are not a good approximation to our model calculations even at several times the threshold energy. Apparently the hydrogenic approximation underestimates the $3d \rightarrow \epsilon f$ cross section for all energies and overestimates the $3p \rightarrow \epsilon d$ cross section for energies up to about several times the threshold energy. Since $l \rightarrow l+1$ transitions represent the bulk of the cross section for ionization of $3d$ and $3p$ subshells these compensating effects can produce a moderately realistic estimate of the cross section in certain spectral ranges.

Note that, as expected, deviations of our model from the hydrogenic approximation become less with

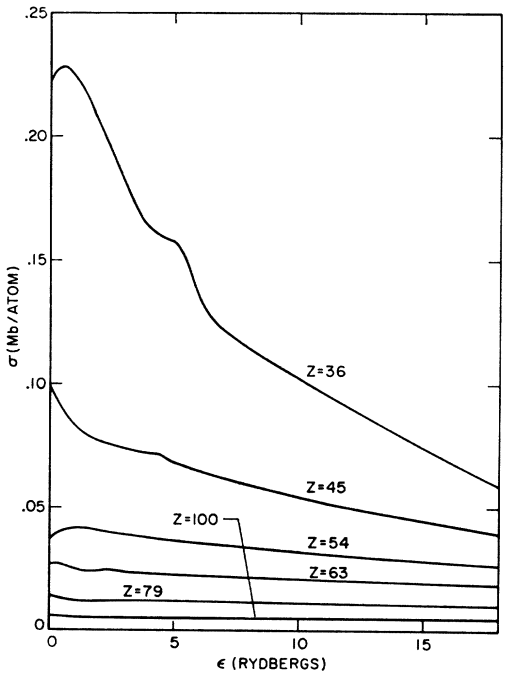

FIG. 10. The $3p \rightarrow \epsilon s$ partial cross sections for Kr, Rh, Xe, Eu, Au, and Fm.

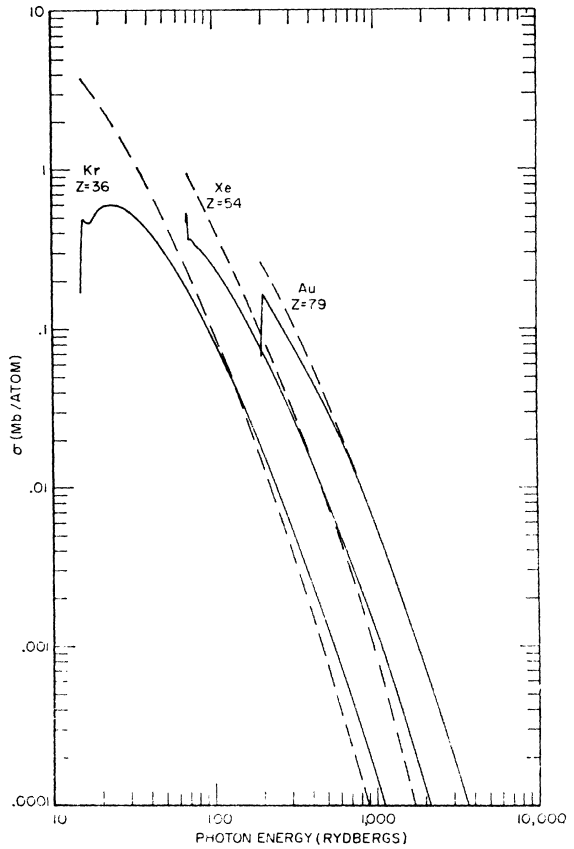

FIG. 11. The $3p \rightarrow \epsilon d$ partial cross sections for Kr, Xe, and Au on a log-log scale. The solid curves are our results and the dashed are the hydrogenic results.

increasing Z. However, substantial deviations both in magnitude and spectral shape are apparent even for Au and those deviations are much larger than those reported for the K shell of Al in Sec. II. This comparison made above casts considerable doubt on the reliability of the hydrogenic approximation for photoeffect cross sections involving M shell electrons even at relatively high energies (say up to ~10 keV).

V. FURTHER DISCUSSION AND RESULTS

In Sec. II we discussed the energy dependence of a photo-ionization matrix element, $R_{\epsilon,l\pm1}$, as being due to two independent factors: a normalization (or enhancement) factor, $C_{l\pm1}(\epsilon)$ and an overlap factor, $\bar{R}_{\epsilon,l\pm1}$. The overlap factor $\bar{R}_{\epsilon,l\pm1}$ was expected to be almost constant over a wide range of energies for interior subshells. The validity of this assumption is illustrated in Table IV which shows $\bar{R}_{\epsilon,l\pm1}$ as a function of energy for the $3d \rightarrow \epsilon f$ transition in gold and fermium. The unnormalized $3d \rightarrow \epsilon f$ matrix element in Fm changes by about 10% over a 16 Ry energy range, while in Au, where the $3d$ shell is not as close to the nucleus as in Fm, $\bar{R}_{\epsilon,l+1}$ changes by more than 20% over the same energy range.

TABLE IV. Unnormalized matrix element $\bar{R}_{\epsilon,l+1}$ for the $3d \rightarrow \epsilon f$ transition in gold and fermium.

Energy (Ry above threshold)	$10^5 \bar{R}$ Au	Fm
0	0.68	0.101
1	0.67	0.100
2	0.66	0.099
4	0.64	0.097
4	0.64	0.097
8	0.60	0.094
16	0.54	0.089

Since the Herman-Skillman potential is the same for all electrons in a given atom, the final states for the photo-ionization of an nl subshell at energy ϵ above threshold are the same as those for an $n'l$ subshell ϵ above its threshold. Thus $C_{l\pm1}(\epsilon)$ is the same for all subshells of the same l in an atom within the framework of our model. This implies that, apart from an energy factor, $\epsilon - \epsilon_{nl}$, the differences in the photo-ionization cross section from various subshells of an atom are due to the differences in overlap, i.e., $\bar{R}_{\epsilon,l\pm1}$. To illustrate

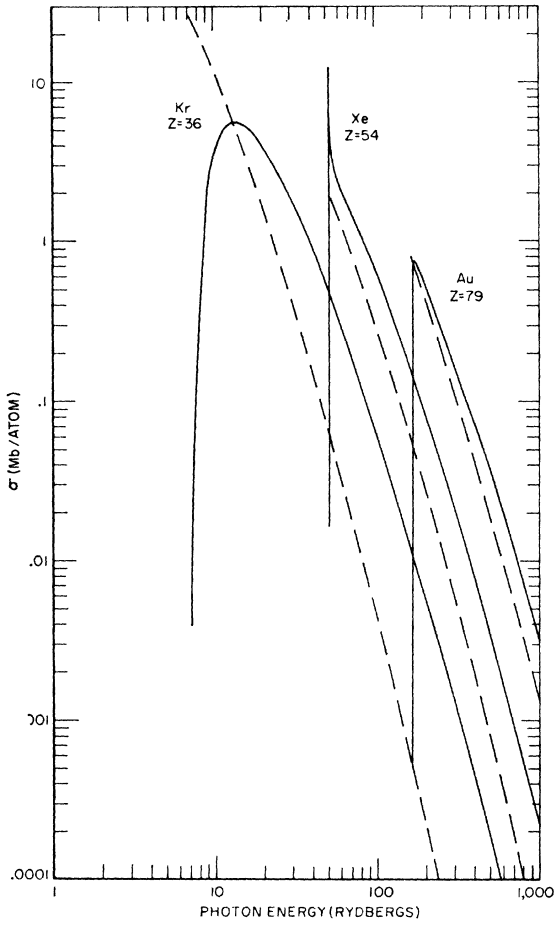

FIG. 12. The $3d \rightarrow \epsilon f$ partial cross sections for Kr, Xe, and Au on a log-log scale. The solid curves are our results and the dashed are the hydrogenic results.

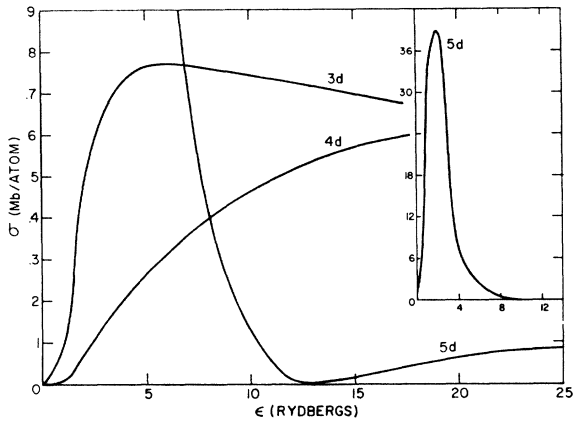

FIG. 13. The $nd \rightarrow \epsilon f$ partial cross sections for $n=3$, 4, 5, in Au.

this we have plotted the $nd \rightarrow \epsilon f$ cross sections in Au for $n=3$, 4, 5 in Fig. 13 and the $np \rightarrow \epsilon d$ in Xe for $n=3, 4, 5$ in Fig. 14. In gold, the $3d \rightarrow \epsilon f$ spectral shape is determined almost entirely by the normalization constant, the $4d \rightarrow \epsilon f$ deviates considerably from this shape indicating the importance of overlap, and the $5d \rightarrow \epsilon f$ is critically dependent upon overlap, $\bar{R}_{\epsilon,l\pm1}$ for this case vanishing at 12.3 Ry above threshold. The xenon $p \rightarrow d$ transitions also exhibit this behavior.

The cross sections of the M_I, N_I, and O_I subshells in Ar, Kr, and Xe are shown in Fig. 15. They are all small at threshold and rise to their maximum values 30–35 eV above threshold. It is well known that the photo-ionization cross section for the valence electron in an alkali[40] (excepting lithium) decreases from threshold to a zero and subsequently reaches a second maximum, as in the case of sodium also shown in Fig. 15. With increasing Z then, the potential becomes stronger and the sign reversal of the matrix element occurs in the discrete, somewhat below threshold, giving rise to the spectral shapes shown in Fig. 15. The $ns \rightarrow \epsilon p$ cross sections shown for the rare gases are much larger than the same cross sections in the alkalis since two electrons are present in a complete $(ns)^2$ subshell and also because practically all of the valence shell oscillator strengths in the alkali is contained in the resonant $ns \rightarrow np$ transition. We expect on the basis of these results that, in general, the cross sections for M_I, N_I, and O_I subshells for most elements will be small very close to threshold and rise quickly to a maximum. Experimental confirmation of this would be desirable.

While we have not investigated in detail the behavior of the K and L_I subshell cross sections we expect that deviations from the hydrogenic approximation occur for these cross sections near threshold particularly for light elements. Further threoretical work along these lines and comparison with available experimental evidence would be useful.

[40] R. D. Hudson, Phys. Rev. **135**, A1212 (1964); R. D. Hudson and V. L. Carter, *ibid.* **139**, A1426 (1965).

VI. FINAL REMARKS

The results presented in the previous sections indicate that calculations within a realistic central-field approximation provide a reasonably accurate first-order approximation of the photo-ionization process and that the joint energy and Z dependence of photo-ionization cross sections, although complex, exhibits certain regularities. These results are expected to be useful both for interpreting the results of future experiments and for providing information on cross sections for materials that cannot be measured. In particular, comparison of calculated cross sections such as those presented here with experiments performed on solid materials in the soft x-ray range is expected to provide valuable information on the properties of solids.

The calculations discussed in this paper are nonrelativistic. Since the primary purpose of this paper is to provide information on the spectral behavior of cross sections at low energies (below 2 keV) the neglect of relativistic effects is not expected to modify any of the results we obtain by more than a few percent. Recent work[31,41,42] on photoeffect at higher energies incorporates both relativistic effects and screened potentials comparable to ours. However, the near threshold behavior of photoeffect cross sections at higher energies, which should be similar to the results obtained here, has not been explored. Further it is not certain in what energy ranges the much more complicated relativistic calculations are necessary to provide reasonably accurate

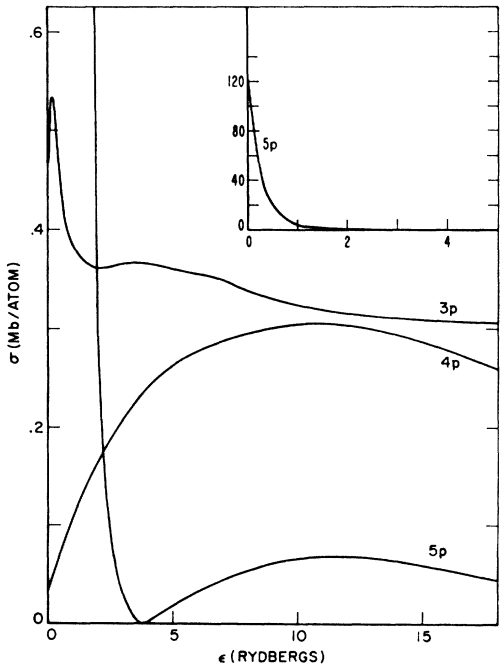

FIG. 14. The $np \rightarrow \epsilon d$ partial cross sections for $n=3$, 4, 5 in Xe.

[41] G. Rakavy and A. Ron, Phys. Rev. **159**, 50 (1964).
[42] R. D. Schmickley and R. H. Pratt, Phys. Rev. **164**, 104 (1967).

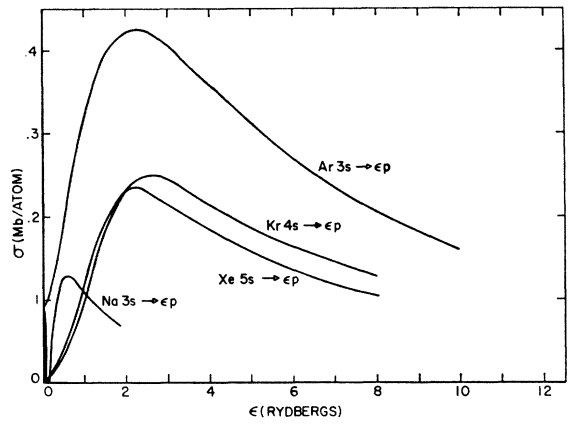

FIG. 15. The $ns \rightarrow \epsilon p$ cross sections for the outermost s-subshell in Na, Ar, Kr, and Xe.

cross sections. Further work along these lines would be valuable.

One of the practical aspects of central-field calculations such as are presented here is that they can be extended to any atomic system in any energy range with relatively little effort.[43] Further calculations of this type are then expected to play an important role in future studies since they provide a useful starting point both for the interpretation of experimental data and for theoretical developments.

Our results also indicate that additional work along the lines followed here would be valuable. Even though our investigation stressed the behavior of the $3p$ and $3d$ subshell contributions, the behavior of the cross sections for these subshells in the transition regions ($Z \cong 24$, 42, and 63) cannot be predicted from the results presented in this paper. Further, while we expect that cross sections calculated with realistic central fields become approximately equal to those of the hydrogenic model (with no inner screening) at high enough energies we have not investigated the high-energy behavior of our calculated cross sections in detail. Further work is needed to shed light on these questions as well as to investigate the properties of other subshell contributions to photo-ionization.

The cross sections reported here may, as mentioned in Sec. I, be considerably in error near thresholds. More realistic calculations may be made by explicitly considering the effects of electron exchange and correlation. This may be done by representing the final state as a solution of a Hartree-Fock equation for a single electron moving in the potential of the ionic core as has been done for outer subshells[44] by expanding both initial and final states as superpositions of the central-field wave functions used here[45] or by an alternative formulation of the problem.[46] While all three approaches lead to improved cross sections near threshold not enough work has been done to give a definitive prescription for estimating effects neglected in a central-field treatment. Further, all of these methods ignore the effects of intershell correlation in the cross section. Recent calculations,[47] as well as the experiments of Ref. 12, indicate that these effects may be important.

ACKNOWLEDGMENTS

We would like to thank Dr. U. Fano and Dr. R. Deslattes for their interest and encouragement during the course of this work.

[43] All of the results reported in this paper represent less than 20 hours computing time on an IBM 7094 computer. Since the work reported here is exploratory in nature, little effort was made to optimize the numerical techniques used in these calculations.

[44] R. J. W. Henry and L. Lipsky, Phys. Rev. **153**, 51 (1967).

[45] An attempt in this direction has been made for $(ns)^2$ subshells. See P. L. Altick and A. E. Glassgold, Phys. Rev. **133**, A632 (1964).

[46] W. Brandt, L. Eder and S. Lundquist, J. Quant. Spectry. Radiative Transfer **7**, 185 (1967).

[47] L. Lipsky and J. W. Cooper (to be published).